International Journal of Applied Mechanics
Vol. 9, No. 6 (2017) 1750088 (20 pages)

DOI: 10.1142/S1758825117500880

World Scientific
www.worldscientific.com

Wavelet Decompositions for High Frequency Vibrational Analyses of Plates

Su Zhang and Li Cheng*

Department of Mechanical Engineering
The Hong Kong Polytechnic University
Hung Hom, Kowloon, Hong Kong SAR, P. R. China
**li.cheng@polyu.edu.hk*

Received 22 April 2017
Revised 10 July 2017
Accepted 11 July 2017
Published 13 September 2017

A wavelet-decomposed Rayleigh–Ritz model for 2D plate vibration analyses is proposed in this work. For an elastically-supported rectangular plate under Love–Kirchhoff theory, 2D Daubechies wavelet scale functions are used as the admissible functions for analyzing the flexural displacement in an extremely large frequency range. For constructing the mass and stiffness matrices of the system, the 2D wavelet connection coefficients are deduced. It is shown that by inheriting the versatility of the Rayleigh–Ritz approach and the superior fitting ability of the wavelets, the proposed method allows reaching very high frequencies. Validations are carried out in terms of both eigen-frequencies and the forced vibration responses for cases which allow analytical solutions. Effects of the wavelet parameters on the calculation accuracy and convergence are also studied.

Keywords: High frequency; Rayleigh–Ritz; wavelet decomposition.

1. Introduction

The structural vibration analysis covering a broad frequency range is a subject of growing importance for numerous applications. For example, with the advent of modern technologies in developing artificially engineered structures, exemplified by acoustic metamaterials [Ang *et al.*, 2016], periodic structures [Zhou *et al.*, 2013; Gao *et al.*, 20l6] and acoustic black hole structures [Zhou *et al.*, 2017], etc., eminent technical challenges are created, among which is the need of reaching higher frequencies with shorter wavelengths due to the lattice effect of the structure. As demonstrated in the open literature, major difficulties reside in the high frequency range due to the lack of accurate, unified and numerically stable methods [Langley and Bardell, 1998]. Two bottle-necking problems arise. First, the reducing structural wavelengths as the frequency increases require more structural details to be considered. Classical finite element methods (FEMs), however, can hardly accommodate

*Corresponding author.

this, since the use of a minimum number of elements per wavelength quickly leads to a large system size and consequently tremendous computational cost [Marburg, 2002]. Pushing the FEM to its high-frequency limit using very high order interpolation functions is also shown to be insufficient [Bardell, 1991; Berry *et al.*, 1992; Carrie and Webb, 1997; Ruta, 1999]. Secondly, high-frequency vibration computation usually suffers from the round-off errors of the computers, accompanied by the inevitable ill-conditioned problem. Therefore, there is a real need for developing methods which allow the prediction of the high frequency vibrations of structures, and the topic is technically challenging.

Among existing semi-analytical methods based on spatial discretization [Cheng and Nicolas, 1992], Rayleigh–Ritz method using artificial spring treatment is probably the most popular one [Cheng and Lapointe, 1995]. In Rayleigh–Ritz approach, the properties of the basis functions significantly affect the computational efficiency, stability and accuracy. It has been demonstrated [Zhang and Cheng, 2016] that various forms of polynomials, constructed from Jacobi polynomials [Carrie and Webb, 1997], Legendre polynomials [Bardell, 1991] or the natural Taylor's basis [Berry *et al.*, 1992], all suffer from the ill-conditioned problems in the calculations of the high-order polynomial coefficients due to the round-off errors of the computers. Trigonometric functions, used as an alternative, suffer from the potential convergence problems at the boundary [Li and Daniels, 2002] due to the well-known Gibbs phenomenon. There has been a consistent effort in exploring ways to choose admissible functions to accommodate the need of various physical problems [Zheng and Wei, 2013; Su *et al.*, 2015].

Wavelets, which are proposed to be investigated in this paper, are expected to provide a solution to overcome the above problems. Apart from their traditional use in signal processing and analyses [Niccoleau and Vassilicos, 2014], wavelets have been used to solve partial differential equations (PDEs) in various fields. Wavelets feature compact support, flexible scaling and translation, and the ability to express any square integrable functions on the real axis [Zhang and Cheng, 2015]. These unique and appealing properties enabled their use to solve various engineering problems [Cohen, 2003] such as the preconditioning of large discretized PDEs [Chen, 1998; Ford and Chen, 2001; Tran *et al.*, 1998]; the adaptive approximation of functions to resolve isolated singularities at a low computational cost [Chen *et al.*, 2006; de Lautour, 1999; Gantumur and Stevenson, 2006] and the sparse representation of the discretized integral equations [Castrillon-Candas and Amaratunga, 2003; Tausch and White, 2003]. Most of the past attempts, however, were made under the FEM framework [Pan *et al.*, 2003], thus inhibiting the shortcomings of the FEM itself. Meanwhile, wavelet functions have also been used as the interpolation functions under the FEM/BEM framework [Geng *et al.*, 2017; Mutinda and Cristinel, 2015]. FEM/BEM discretizes the structural domain and approximates the solution using local interpolation basis functions. They all embrace the common philosophy of the so-called local expansion.

Using a Euler–Bernoulli beam, our previous work [Zhang and Cheng, 2016] demonstrated the efficacy of a wavelet-decomposed Rayleigh–Ritz method (WDRM) for high-frequency vibration analyses of 1D structures. It has been shown that the localized compact support properties of the wavelets lead to a sparse representation of the system matrices. Along with their exceptional fitting ability and the tactic treatment of the structural boundary using artificial springs, the WDRM approach exhibits tremendous computational advantages and allows reaching extremely high frequency range in 1D cases. As compared to the conventional FEM/BEM method, expansion of the displacement over the entire structural span can be referred to as global expansion method.

This paper extends the previous work on 1D structure to 2D planar cases. Among other technical aspects, the handling of the 2D Daubechies wavelet scale functions presents particular challenges. To the best of our knowledge, very few papers attempt the high frequency plate analyses, with the exception of the work [Beslin and Nicolas, 1997] in which structural modes in what can be regarded as the mid-frequency range were investigated. The use of 2D Daubechies wavelets as the global basis for plate problems has not yet been investigated up to now. The objective of this paper is twofold: (1) to demonstrate the efficacy of the wavelet-decomposed method in dealing with the high frequency vibration problems of plates; and (2) to solve the problem of the connection coefficients of 2D Daubechies wavelet scale functions. The latter becomes challenging due to the strong oscillation nature of the Daubechies wavelets and the lack of the closed-form expressions.

The outline of the paper is as follows. Section 2 describes the theoretical modeling framework. 2D Daubechies wavelet scaling functions are briefly recalled and the calculation method of the 2D connection coefficients are presented. Numerical results are given and discussed in Sec. 3. Whenever possible, comparisons with analytical results are carried out for validations and assessment. The convergence properties of the algorithm on relation to the parameters of the wavelet functions are investigated. Both free and forced vibration analyses cover a large frequency band, containing typically thousands of structural modes.

2. Theory

2.1. *Plate model*

Consider a flat rectangular plate shown in Fig. 1(a), bounded along its edges by $x = 0$, $x = a$ and $y = 0$, $y = b$. The elastically-supported plate is assumed to be isotropic, homogeneous and subjected to small displacement assumptions, allowing the decoupling of the bending and in-plane motions when undergoing out-of-plane vibrations. For illustration purposes, the Love–Kirchhoff theory is used. Note the use of other more accurate plate theories considering shear effect and the rotational energy should not pose any particular technical difficulties. The displacement field

for the plate is written as

$$\{u, v, w\} = \left\{-z\frac{\partial w}{\partial x}, -z\frac{\partial w}{\partial y}, w(x, y, t)\right\}. \tag{1}$$

The x and y coordinates are normalized by

$$\xi = x/a, \quad \eta = y/b. \tag{2}$$

The transverse displacement, w, is expressed as

$$w(\xi, \eta, t) = \sum_{m=1}^{M}\sum_{n=1}^{N} q_{mn}(t) f_m(\xi) f_n(\eta), \tag{3}$$

where $f_m(\xi)$ and $f_n(\eta)$ are the assumed admissible functions and $q_{mn}(t)$ the time-dependent unknowns to be determined.

The plates are elastically supported by a set of artificial translational and rotational springs, which are continuously and uniformly distributed along its edges with different stiffnesses (k_i in N/m for the translation and k_{θ_i} in N/rad for the rotation with $i = 1, 2, 3, 4$), shown in Fig. 1(b). Adjusting the stiffness values of the springs allows the representation of various boundary conditions [Langley and Bardell, 1998]. For example, simply-supported boundaries can be obtained by using a sufficiently large k_i and a zero k_{θ_i}.

Rayleigh–Ritz procedure requires the construction of various energy terms of the system. Lagrange's equations can then be applied to find the stationary state of the Hamiltonian with $q_{mn}(t)$ as the generalized coordinates

$$\frac{d}{dt}\left(\frac{\partial L}{\partial \dot{q}_{mn}(t)}\right) - \frac{\partial L}{\partial q_{mn}(t)} = 0, \quad (m = 0, 1, 2, \ldots, r \text{ and } n = 0, 1, 2, \ldots, s), \tag{4}$$

where L is the Lagrangian of the system expressed as

$$L = E_k - E_p + W, \tag{5}$$

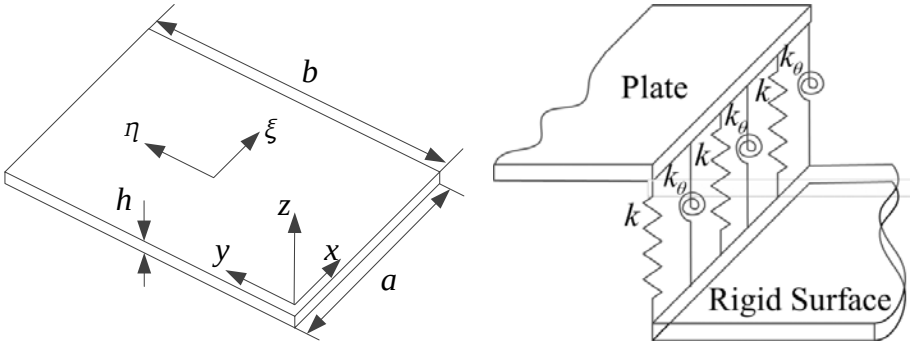

(a) (b)

Fig. 1. (a) Model of a rectangular plate. (b) Artificial springs along the boundary.

where the kinetic energy E_k, potential energy E_p, and the work W done by the external excitation force is written as

$$E_k = \frac{\rho ab}{2}\int_0^1\int_0^1 \left(\frac{\partial w}{\partial t}\right)^2 d\xi d\eta, \tag{6}$$

$$\begin{aligned} E_p = {} & \frac{D}{2ab}\int_0^1\int_0^1 \left[\frac{b^2}{a^2}\left(\frac{\partial^2 w}{\partial \xi^2}\right)^2 + \frac{a^2}{b^2}\left(\frac{\partial^2 w}{\partial \eta^2}\right)^2,\right. \\ & \left. + 2v\left(\frac{\partial^2 w}{\partial \xi^2}\right)\left(\frac{\partial^2 w}{\partial \eta^2}\right) + 2(1-v)\left(\frac{\partial^2 w}{\partial \xi \partial \eta}\right)^2\right] d\xi d\eta \\ & + \frac{b}{2}\int_0^1 \left\{k_1[w(\xi,\eta,t)|_{\xi=0}]^2 + k_2[w(\xi,\eta,t)|_{\xi=1}]^2\right. \\ & \left. + \frac{k_{\theta_1}}{a^2}\left[\frac{\partial w(\xi,\eta,t)}{\partial \xi}|_{\xi=0}\right]^2 + \frac{k_{\theta_2}}{a^2}\left[\frac{\partial w(\xi,\eta,t)}{\partial \xi}|_{\xi=1}\right]^2\right\} d\eta \\ & + \frac{a}{2}\int_0^1 \left\{k_3[w(\xi,\eta,t)|_{\eta=0}]^2 + k_4[w(\xi,\eta,t)|_{\eta=1}]^2\right. \\ & \left. + \frac{k_{\theta_3}}{b^2}\left[\frac{\partial w(\xi,\eta,t)}{\partial \xi}|_{\eta=0}\right]^2 + \frac{k_{\theta_4}}{b^2}\left[\frac{\partial w(\xi,\eta,t)}{\partial \xi}|_{\eta=1}\right]^2\right\} d\xi, \end{aligned} \tag{7}$$

where ρ is the density, and $D = Eh^3/12(1-\nu^2)$ is the flexural rigidity.

$$W = \sum_{\delta=1}^{\Delta}[f_\delta(t)w(\xi_\delta,\eta_\delta,t)]. \tag{8}$$

The symbol Δ in Eq. (8) represents the number of forces applied to the system and $(\xi_\delta,\eta_\delta,t)$ the application point of each of them.

Assuming that the transverse motion is harmonic and inserting the w expressions Eq. (3) into Eqs. (6) and (7), and then into Eq. (4), classical eigenvalue problem and forced vibration problem are formed as

$$[K_{ijmn}]\{q_{mn}\} = \omega^2[M_{ijmn}]\{q_{mn}\}, \tag{9}$$

$$[[K_{ijmn}] - \omega^2[M_{ijmn}]]\{q_{mn}\} = \{F\}, \tag{10}$$

where $[M]$ and $[K]$ are the mass and stiffness matrices, respectively, with

$$M_{ijmn} = \rho hab I^{0,0}_{i,m} J^{0,0}_{j,n}, \tag{11}$$

$$\begin{aligned} K_{ijmn} = {} & \frac{D}{ab}\left[\left(\frac{b^2}{a^2}\right) I^{2,2}_{i,m} J^{0,0}_{j,n} + \left(\frac{a^2}{b^2}\right) I^{0,0}_{i,m} J^{2,2}_{j,n}\right. \\ & \left. + v(I^{2,0}_{i,m} J^{0,2}_{j,n} + I^{0,2}_{i,m} J^{2,0}_{j,n}) + 2(1-v) I^{1,1}_{i,m} J^{1,1}_{j,n}\right], \end{aligned} \tag{12}$$

$$F_{ij} = \sum_{\delta=1}^{\Delta} F_\delta(t) f_i(\xi_\delta) f_j(\eta_\delta), \tag{13}$$

in which

$$I_{i,m}^{\alpha,\beta} = \int_0^1 f_i^\alpha(\xi) f_m^\beta(\xi) d\xi, \quad J_{j,n}^{\alpha,\beta} = \int_0^1 f_j^\alpha(\eta) f_n^\beta(\eta) d\eta, \tag{14}$$

where the indices α and β ($\alpha, \beta = 0, 1, 2$) denote the order of the derivatives.

The above integrals can be calculated using the Gaussian quadrature method with an appropriate number of integration points for the function in the integrand of each integral. The resulting values of the integrals, once calculated, can be stocked into a file for the generation of the stiffness and mass matrices.

2.2. *Wavelet decomposition*

2.2.1. *2D Daubechies wavelets scaling functions*

1D Daubechies wavelets scaling functions are governed by a set of L (an even integer) coefficients $\{h_j : j = 0, 1, \ldots, L-1\}$ through a two-scale relation as

$$\varphi(x) = \sum_{j=0}^{L-1} h_j \varphi(2x - j), \tag{15}$$

where the coefficients h_j are the wavelet filter coefficients whose values can be found in the literature [Daubechies, 1992]. 2D wavelet scaling functions can be constructed as a tensor product of the 1D functions as [Mallat, 1999]

$$\varphi(x, y) = \varphi(x) \otimes \varphi(y), \tag{16}$$

where $\otimes$ is the kronecker symbol.

2.2.2. *Basis construction*

1D wavelet basis, as discussed in a previous work [Zhang and Cheng, 2016], is written as

$$\phi_j(x) = 2^{m/2} \varphi(2^m x - j). \tag{17}$$

To determine a suitable range of j, all the terms between the normalized expansion domain [0, 1] should be included into the expansion set. However, substituting Eq. (17) into Eq. (3) requires the calculation of Eq. (14). As the wavelet scale function is a compact support function, when Eq. (14) equals to zero, the mass and stiffness matrices $\mathbf{M}$ and $\mathbf{K}$ defined by Eqs. (11) and (12) are singular and the problem becomes underdetermined. Therefore, the expansion set Equation (17) should be carefully chosen as below to avoid such occurrence:

$$\phi_j(x) = 2^{m/2} \varphi(2^m x - j), \quad j = -L + 2, \ldots, 2^m - 1. \tag{18}$$

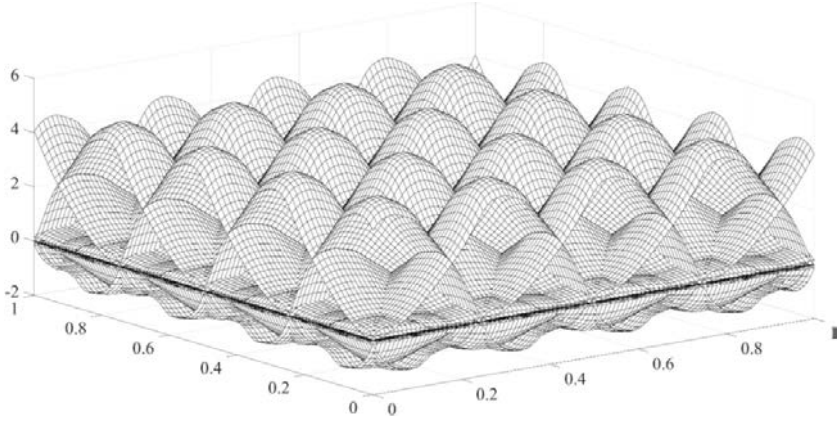

Fig. 2. 2D Daubechies scaling function selection criteria.

In the present 2D situation,

$$\begin{aligned}\phi_j(x) &= 2^{m/2}\varphi(2^m x - j), \quad j = -L+2, \ldots, 2^m - 1,\\ \phi_k(y) &= 2^{m/2}\varphi(2^m y - k), \quad k = -L+2, \ldots, 2^m - 1.\end{aligned} \tag{19}$$

The total number of the decomposition items is $(2^m + L - 2)^2$. For illustration purposes, a typical 2D Daubechies scaling function basis is shown in Fig. 2, with $L = 8$, $m = 2$, $j = -6, \ldots, 3$, $k = -6, \ldots, 3$.

2.2.3. *2D connection coefficients*

Substituting the tensor form of the 2D wavelet scaling function, Eq. (16), into Eq. (3), the mass and stiffness matrices, Eqs. (11) and (12), are converted to

$$\mathbf{M} = \rho hab \bullet \mathbf{I}^{0,0} \otimes \mathbf{I}^{0,0}, \tag{20}$$

$$\begin{aligned}\mathbf{K} = {} & \frac{D}{ab}\left[\left(\frac{b^2}{a^2}\right)\mathbf{I}^{2,2} \otimes \mathbf{I}^{0,0} + \left(\frac{a^2}{b^2}\right)\mathbf{I}^{0,0} \otimes \mathbf{I}^{2,2},\right.\\ & \left. + v(\mathbf{I}^{2,0} \otimes \mathbf{I}^{0,2} + \mathbf{I}^{0,2} \otimes \mathbf{I}^{2,0}) + 2(1-v)\mathbf{I}^{1,1} \otimes \mathbf{I}^{1,1}\right]\\ & + bk_1\boldsymbol{\varphi}_- \otimes \mathbf{I}^{0,0} + bk_2\boldsymbol{\varphi}_+ \otimes \mathbf{I}^{0,0} + \frac{bk_{\theta_1}}{a^2}\boldsymbol{\varphi'}_- \otimes \mathbf{I}^{0,0} + \frac{bk_{\theta_2}}{a^2}\boldsymbol{\varphi'}_+ \otimes \mathbf{I}^{0,0}\\ & + ak_3\mathbf{I}^{0,0} \otimes \boldsymbol{\varphi}_- + ak_4\mathbf{I}^{0,0} \otimes \boldsymbol{\varphi}_+ + \frac{ak_{\theta_3}}{b^2}\mathbf{I}^{0,0} \otimes \boldsymbol{\varphi'}_- + \frac{ak_{\theta_4}}{b^2}\mathbf{I}^{0,0} \otimes \boldsymbol{\varphi'}_+,\end{aligned} \tag{21}$$

where

$$\begin{aligned}\boldsymbol{\varphi}_- = \{\varphi_i(0)\varphi_j(0)\}, \quad & i = -L+2, -L+1, \ldots, 2^m - 1,\\ & j = -L+2, -L+1, \ldots, 2^m - 1,\end{aligned}$$

$$\begin{aligned}
\boldsymbol{\varphi}_+ &= \{\varphi_i(1)\varphi_j(1)\}, \quad i = -L+2, -L+1, \ldots, 2^m - 1, \\
&\quad j = -L+2, -L+1, \ldots, 2^m - 1, \\
\boldsymbol{\varphi}'_- &= \{\varphi'_i(0)\varphi'_j(0)\}, \quad i = -L+2, -L+1, \ldots, 2^m - 1, \\
&\quad j = -L+2, -L+1, \ldots, 2^m - 1, \\
\boldsymbol{\varphi}'_+ &= \{\varphi'_i(1)\varphi'_j(1)\}, \quad i = -L+2, -L+1, \ldots, 2^m - 1, \\
&\quad j = -L+2, \ -L+1, \ldots, 2^m - 1, \\
\mathbf{F} &= \sum_{\delta=1}^{\Delta} F_\delta \boldsymbol{\varphi}(\xi_\delta, \eta_\delta). \qquad (22)
\end{aligned}$$

Then

$$\mathbf{I}^{\alpha,\beta} = \int_0^1 \boldsymbol{\varphi}_1^{T^{(\alpha)}}(\xi)\boldsymbol{\varphi}_2^{(\beta)}(\xi)d\xi. \qquad (23)$$

Here, the 2D connection coefficients, $\mathbf{I}^{\alpha,\beta}$, are converted to the tensor product of 1D connection coefficients. Substituting Eq. (17) into Eq. (13), one gets

$$\begin{aligned}
I_{i,j}^{\alpha,\beta} &= \int_0^1 [2^{m/2}\varphi(2^m\xi - i)]^{(\alpha)}[2^{m/2}\varphi(2^m\xi - j)]^{(\beta)}d\xi \\
&= 2^{(\alpha+\beta)m}\int_0^{2^m} \varphi^{(\alpha)}(x - i)\varphi^{(\beta)}(x - j)dx. \qquad (24)
\end{aligned}$$

The function form of $\varphi^{(\cdot)}(x - i)$ is the differential of the 1D Daubechies wavelet scaling functions, which can be obtained through a recursive scheme as detailed in our previous work [Zhang and Cheng, 2016]. $\mathbf{I}^{\alpha,\beta}$ can then be calculated by Gauss integration.

3. Numerical Results and Discussions

The following sections consider a rectangular steel plate with different boundary conditions. Again, it is relevant to reiterate that the validity issue of the Love–Kirchhoff assumption in the high-frequency range is well known and beyond the scope of the present paper. The illustration of the computation accuracy of the proposed method through comparison with a simple benchmark problem having exact solutions is the major focus here.

3.1. *Low-order eigenvalue validations*

The eigen-frequency problem described by Eq. (9) is first considered for low-order modes. Three different boundary conditions are investigated using the same notations in [Leissa, 1973]. For example, corresponding to the four edges at $x = 0$, $y = 0$, $x = a$, $y = b$, C-S-C-F denotes clamped, simply-supported, clamped and free

boundaries, respectively. For each type of boundary conditions, results are tabulated by including the first four natural frequencies of the plate for three different aspect radios ($a/b = 2/5, 1, 5/2$), along with the results from other work in the literature. The support length L and the resolution m of the wavelet scale function used in the calculation are also quoted for each case. For the convenience of comparison with results from the literature [Bardell, 1991; Leissa, 1973], a non-dimensional frequency parameter is defined as

$$\Omega = \omega a^2 \sqrt{\rho/D}, \tag{25}$$

where ω is angular frequency and a is the length of the rectangular plate.

Firstly, the accuracy of the WDRM is checked when all four edges of the plate are completely free (F-F-F-F). In this case, the plate boundary conditions are fully accounted for in the original matrix equation with no stiffness values being assigned to the springs. The eigenvalue problem yields three zero frequency parameters (as expected) which correspond to the rigid-body translation and rigid-body rotations. The subsequent non-zero frequency parameters are shown in Table 1.

Table 1. Frequency parameters for a F-F-F-F plate: $L = 18$, $m = 4$.

a/b	Mode No.	Leissa	Bardell	WDRM
2/5	Ω_4	3.463	3.433	3.428
	Ω_5	5.288	5.278	5.275
	Ω_6	9.622	9.541	9.540
	Ω_7	11.437	11.329	11.324
1.0	Ω_4	13.489	13.468	13.465
	Ω_5	19.789	19.596	19.593
	Ω_6	24.432	24.270	24.269
	Ω_7	35.024	34.801	34.799
5/2	Ω_4	21.643	21.454	21.374
	Ω_5	33.050	32.989	32.964
	Ω_6	60.137	59.629	59.602
	Ω_7	71.484	70.804	70.789

Table 2. Frequency parameters for C-C-C-C plate: $L = 18$, $m = 4$.

a/b	Mode No.	Leissa	Bardell	WDRM
2/5	Ω_1	23.65	23.64	23.64
	Ω_2	27.82	27.81	27.80
	Ω_3	35.45	35.44	35.41
	Ω_4	46.70	46.81	46.67
1.0	Ω_1	35.99	35.99	35.99
	Ω_2	73.41	73.39	73.39
	Ω_3	73.41	73.39	73.39
	Ω_4	108.22	108.22	108.21
5/2	Ω_1	147.80	147.78	147.75
	Ω_2	173.85	173.80	173.78
	Ω_3	221.54	221.50	221.33
	Ω_4	291.89	292.53	291.65

Table 3. Frequency parameters for C-S-C-F plate: $L = 18$, $m = 4$.

a/b	Mode No.	Leissa	Bardell	WDRM
2/5	Ω_1	22.54	22.49	22.49
	Ω_2	24.30	24.27	24.26
	Ω_3	28.34	28.32	28.32
	Ω_4	35.35	35.31	35.36
1.0	Ω_1	23.46	23.38	23.38
	Ω_2	35.61	35.56	35.55
	Ω_3	63.13	62.89	62.85
	Ω_4	66.81	66.77	66.68
5/2	Ω_1	28.56	28.49	28.48
	Ω_2	70.56	70.31	70.32
	Ω_3	114.00	113.91	113.79
	Ω_4	130.84	130.53	130.61

As can be seen, for all first four frequencies, WDRM, Lessia's work [Leissa, 1973] and Bardell's work [Bardell, 1991] provide very close results. It should also be noted that the WDRM generates the smallest values for each natural frequency, suggesting a higher accuracy than the other two.

Then, plates with C-C-C-C and C-S-C-F boundary conditions are investigated. The first four frequency parameters are presented in Tables 2 and 3, respectively, for the two boundary cases. Once again, the comparison shows the same tendency as explained before and an excellent agreement is observed with the work of [Leissa, 1973] and [Bardell, 1991]. Meanwhile, the WDRM yields consistently lower frequencies for all cases compared with their counterparts reported in [Leissa, 1973; Bardell, 1991].

3.2. *High order eigenvalues and convergence study*

A simply-supported plate (S-S-S-S) is studied due to the existence of analytical solutions. The geometrical and material parameters of the plate are: $a = 1\,\text{m}$, $b = 1\,\text{m}$, $h = 0.003\,\text{m}$; Young's modulus $E = 2.1 \times 10^{11}\,\text{Pa}$; Poisson ratio $\nu = 0.3$; and density $\rho = 7{,}800\,\text{kg/m}^3$. As an example, the aspect radio a/b is restricted to 1. The translational stiffness terms of the boundary springs are set as $k_1 = k_2 = k_3 = k_4 = 1E12\,\text{N/m}$ and $k_{\theta_1} = k_{\theta_2} = k_{\theta_3} = k_{\theta_4} = 0$. Convergence studies show that further increases in k_i or k_{θ_i} would not lead to noticeable changes in the calculated results.

Convergence and error analyses are carried out. It should be noted that the derivative order of the Daubechies wavelet scaling functions requires the use of a minimum support length L. Theoretically, the maximum differential order of the Daubechies wavelet functions is $(L-2)/2$. In the present plate case, the differential order in the equation of motion is four. Therefore, the minimum L should be ten. Satisfying this criterion, Fig. 3 shows the eigenfrequencies calculated by the WDRM using $L = 14$, $L = 16$ and $L = 18$, respectively, with a fixed resolution $m = 7$, in comparison with the analytical solutions.

To quantify the accuracy, a relative error is defined for each eigen-frequency as

$$\eta = |f_{\text{exact}} - f_{\text{WDRM}}|/f_{\text{exact}} \times 100\%, \tag{26}$$

where f_{exact} is the exact frequency value and f_{WDRM} the numerically calculated one by the WDRM.

The relative error for the same calculation cases ($L = 14$, $L = 16$ and $L = 18$, with $m = 7$) is shown in Fig. 4. Both Figs. 3 and 4 show a consistently good accuracy of the calculation for all cases, typically covering the first 2,000 modes (Fig. 4). Errors start to increase for higher-order modes. If the calculation error is capped at 1%, $L = 14$, $L = 16$, and $L = 18$ with $m = 7$ allow the correct prediction of the first 2,300, 2,800 and 3,500 modes, respectively (Fig. 4). The corresponding basis

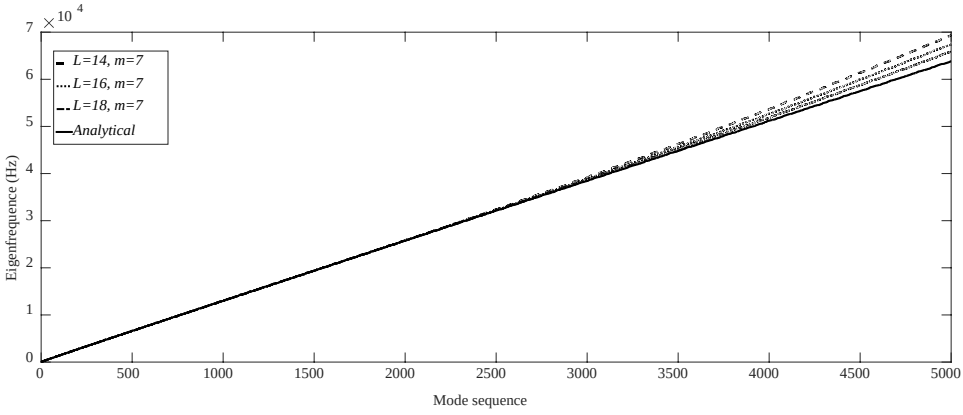

Fig. 3. Eigenfrequencies using different wavelet support lengths $L = 14$ (dashed line), $L = 16$ (dotted line) and $L = 18$ (dashed-dotted line) with the wavelet resolution m being fixed at 7, in comparison with analytical ones (solid line).

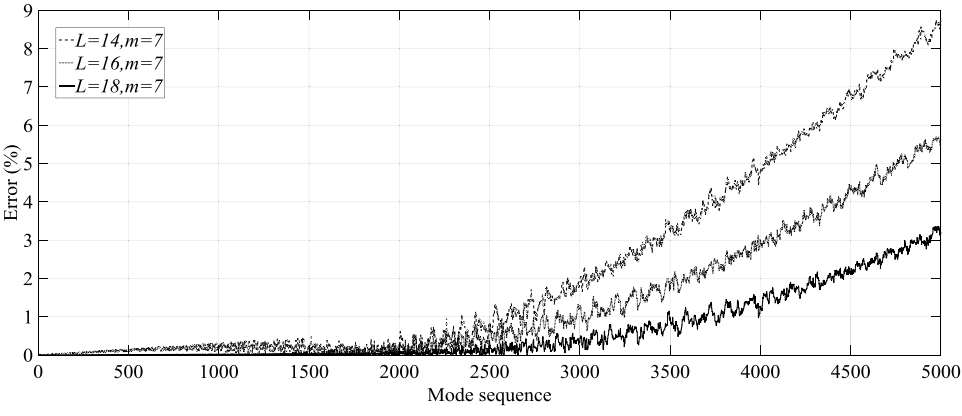

Fig. 4. Relative error using different wavelet support lengths $L = 14$ (dashed line), $L = 16$ (dotted line) and $L = 18$ (solid line) with the wavelet resolution m fixed at 7.

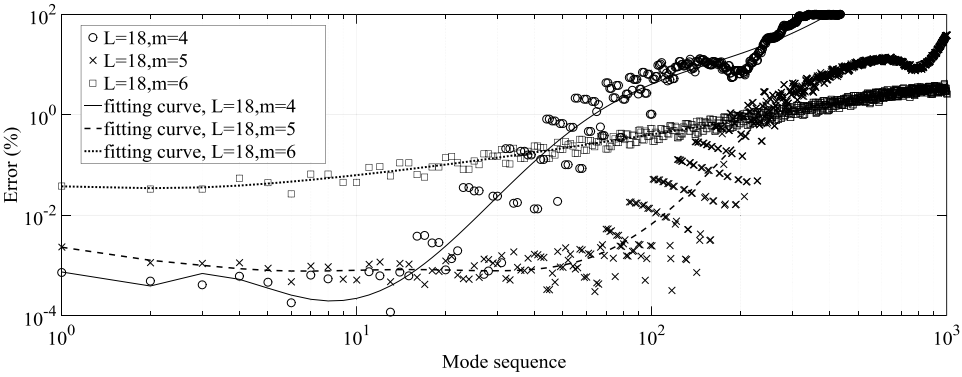

Fig. 5. Relative error using different wavelet resolutions $m = 4$ (dotted line), $m = 5$ (dotted) and $m = 6$ (dashed) with the wavelet support length L fixed at 18 from 1st mode to 1,000th mode.

terms used are 19,600, 20,614 and 20,736, respectively. Obviously, the calculation accuracy, along with the frequency coverage, increases with the support length.

When varying the resolution parameter m, the relative error is shown in Figs. 5 and 6. As can be seen from Fig. 5, m needs to be increased for the same support length L for more modes to be correctly calculated. More specifically, when $m = 4$, about 70 eigen-frequencies can be obtained under 1% error. This number increases to about 200 when $m = 5$; and 300 when $m = 6$, respectively. For relatively small m values, the improvement in terms of frequency coverage is rather gentle. Further increasing m, Fig. 6 shows that, when $m = 7$, about 3,400 eigen-frequencies can be obtained under 1% error. This number increases to about 15,000 when $m = 8$. Therefore, the effect of the resolution parameter m is obvious. When m increases up to a certain value, the accuracy of the WDRM is improved in a significant manner. Note that, for the sake of convenience, the lower order modes, with their error values all below 1%, are not shown in Fig. 6.

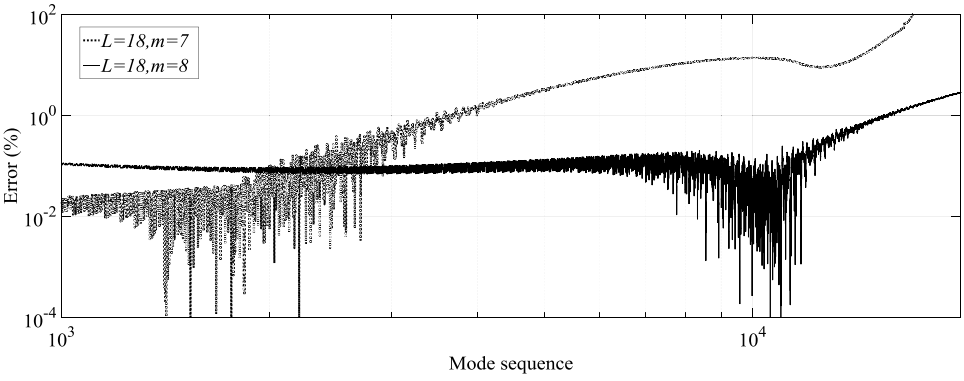

Fig. 6. Relative error using different wavelet resolutions $m = 7$ (dotted line) and $m = 8$ (solid) and with the wavelet support length L fixed at 18 from 1,000th mode to 20,000th mode.

Another phenomenon is noteworthy from Figs. 5 and 6. Although the accuracy generally increases with m, it does not mean that a larger m is necessarily better for any specified mode sequence range. To show the phenomenon more clearly, a tendency line on the relative error curves is plotted in Fig. 5. For the mode sequence from the 1st to about the 15th, the most accurate result is obtained using $m = 4$. From the 16th to the 200th modes, the smallest relative error is obtained using $m = 5$. The same phenomenon can be again observed in Fig. 6, in which $m = 7$ gives the most accurate prediction accuracy for the mode sequence from the 1,000th to about the 2,000th. A plausible explanation is that the different mode involves different structural wavelengths. There should exist some correlations between the structural wavelength range of the modes and the wavelet resolution m. If the calculation is to be conducted by targeting a particular range, a smaller m may generate better accuracy for the lower-order modes. Higher-order modes, however, requires the use of a larger m.

In the present case with $L = 18$, $m = 6$, the CPU time is about 620 s for the whole calculation. Generally speaking, the CPU time is related to $(2^m + L - 2)^2$ according to Eq. (19), which is the size of the mass and stiffness matrices.

In Fig. 7, the first four mode shapes of the S-S-S-S plate using the WDRM with $L = 18$ and $m = 7$ are presented. It can be seen that, despite the seemingly strong oscillation feature of the wavelets, the lower-order mode shapes are well constructed in a continuous and smooth manner.

As another extreme example, two arbitrarily chosen high-order mode shapes (the 2,592nd at 36,741 Hz and the 2,822nd at 39,619 Hz) of the S-S-S-S plate using

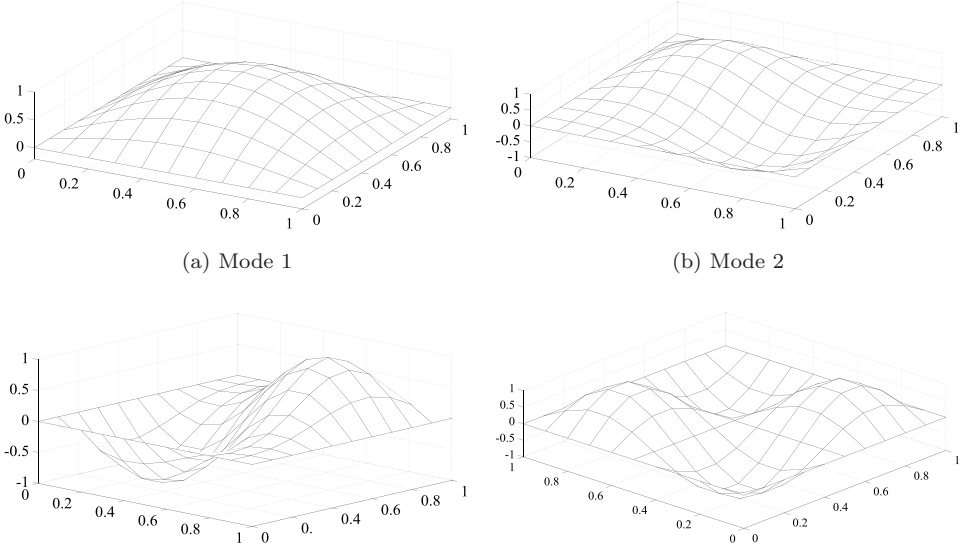

(a) Mode 1 (b) Mode 2

(c) Mode 3 (d) Mode 4

Fig. 7. The first four mode shapes calculated by the WDRM.

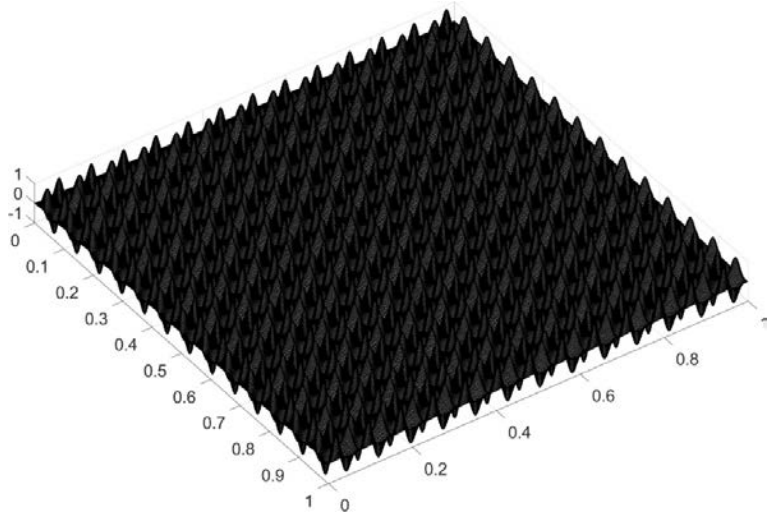

(a)

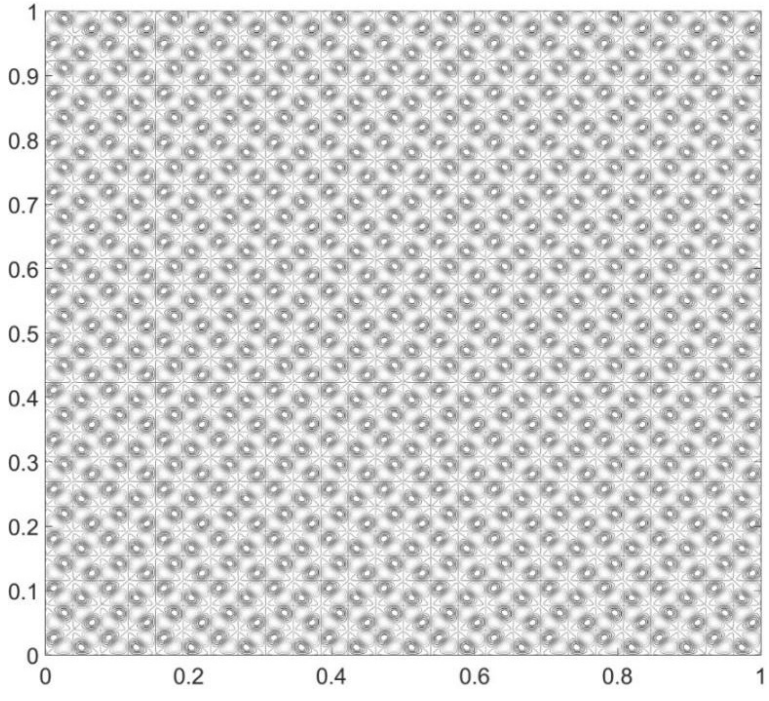

(b)

Fig. 8. Mode shape of the 2,592nd mode of the S-S-S-S plate using the WDRM. (a) 3D view. (b) Top contour view.

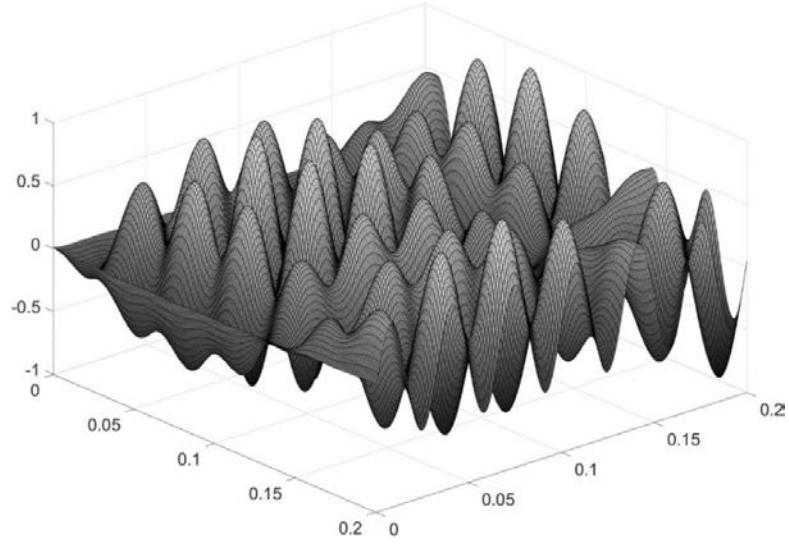

(a)

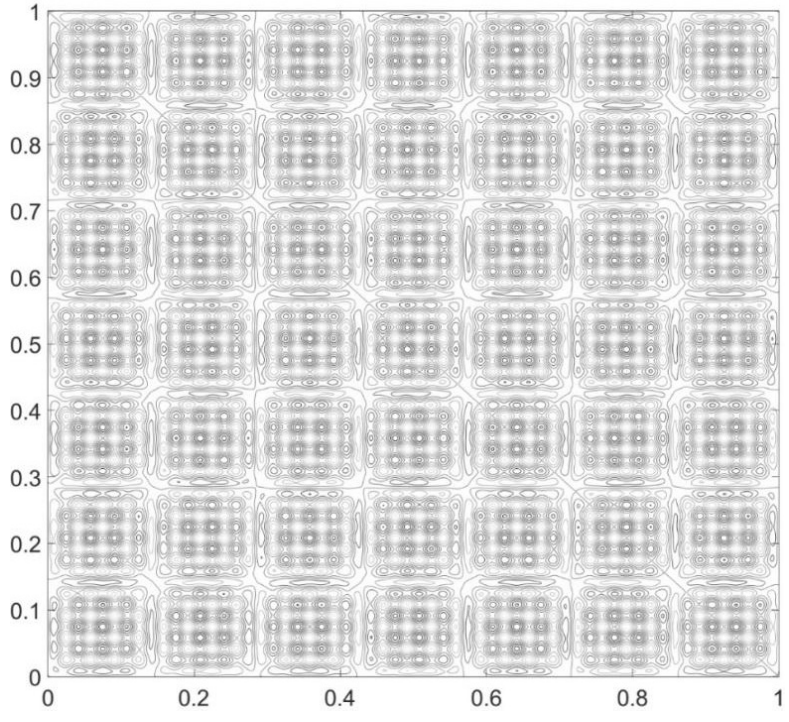

(b)

Fig. 9. Mode shape of the 2,822nd mode of the S-S-S-S plate using the WDRM. (a) Partial 3D view. (b) Top contour view.

the WDRM are depicted in Figs. 8 and 9, respectively, together with the corresponding top views. Note that, for the 2,822nd mode, only a small portion of the plate (1/5 in each directions) is shown in the 3D view in order to better illustrate details. It can be seen from these figures that these high-order mode shapes are also well predicted with fine details and smoothness even near the edges, demonstrating the strong ability of the wavelet-decomposed model in coping with structural details.

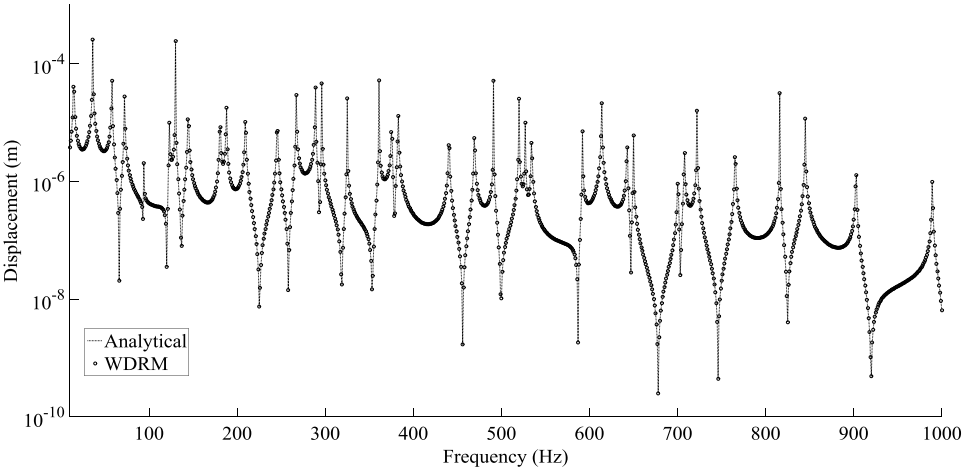

(a)

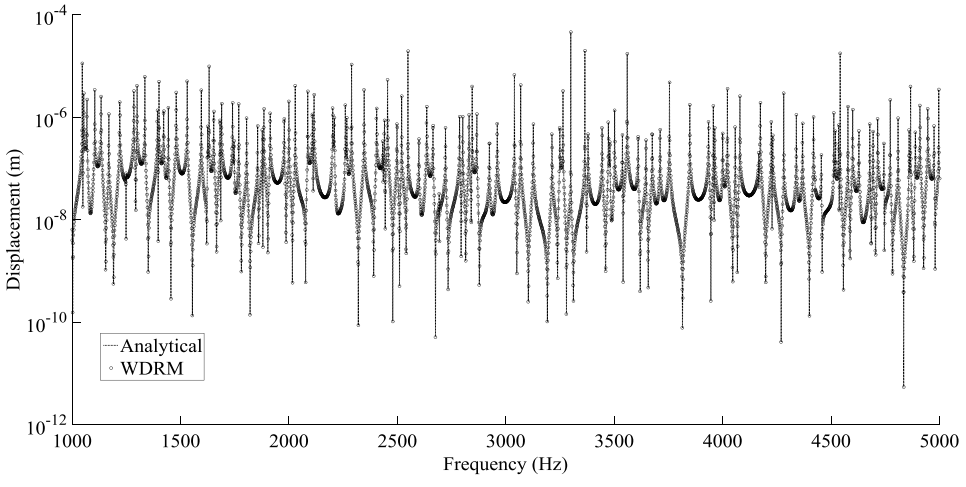

(b)

Fig. 10. Displacement amplitude at (0.75 m, 0.6 m) in three different frequency bands: (a) from 10 Hz to 1k Hz, (b) from 1 kHz to 5 kHz, (c) from 5 kHz to 10 kHz.

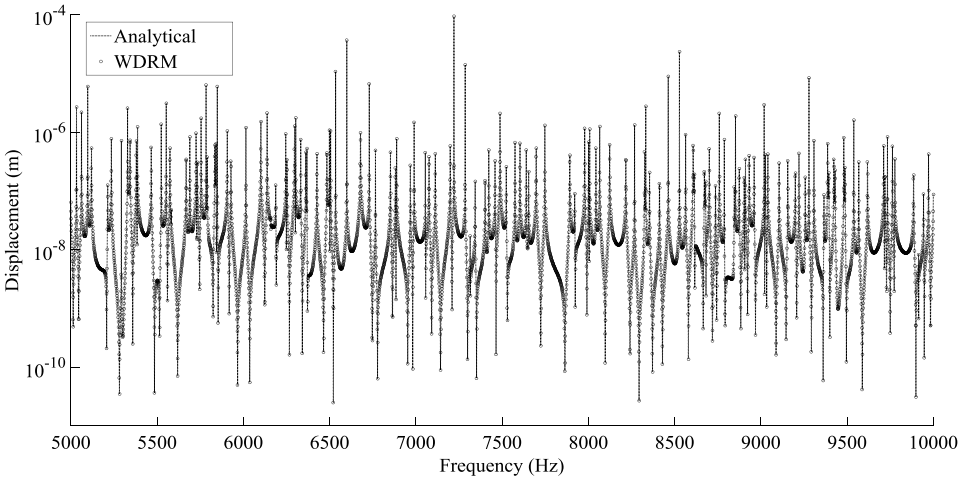

(c)

Fig. 10. (*Continued*)

3.3. *Forced vibrations*

The forced vibration response of the S-S-S-S plate is investigated to further verify the accuracy of the proposed method. The geometrical and material parameters of the plate remain the same as before. System damping is ignored. A unit excitation force is applied at an arbitrarily chosen point at (0.1 m, 0.2 m). The displacement of the plate at another arbitrarily chosen location (0.75 m, 0.6 m) is calculated and shown in Fig. 10, in a frequency range from 10 Hz to 10 kHz. Calculations use $L = 18$ and $m = 7$. The analytical solution [Rao, 2007] is used as the reference, in which one million modes were used. In all three frequency bands, low in Fig. 10(a), middle in Fig. 10(b) and high in Fig. 10(c), the displacement responses calculated by the WDRM are found to be in nice agreement with the analytical solutions, demonstrating again the remarkable accuracy of the method, even for very high frequencies.

4. Conclusions

2D Daubechies wavelet scaling functions are used under the general framework of Rayleigh–Ritz method for analyzing the high-frequency bending vibrations of plates. Upon constructing the 2D Daubechies wavelet scaling functions and establishing the calculation scheme for the associated 2D connection coefficients, a wavelet-decomposed Rayleigh–Ritz plate model is developed. By embracing the flexibility of the global methods and the accuracy of local methods, and exploiting the versatility of the Rayleigh–Ritz approach and the unique features of the wavelets, the proposed method exhibits extraordinary computational advantages and allows reaching

extremely high frequencies with conventional computational facilities. Typically, upon properly choosing the wavelet parameters, the plate vibration, in both free and forced regimes, can be accurately simulated, covering roughly fifteen thousand plate modes. Typical errors of the calculated natural frequencies are capped at 1%. Numerical analyses also allow shedding light on the relationship among the accuracy, convergence of the calculations and the wavelet parameters, namely the support length L and the resolution m. In general, the calculation accuracy increases with the support length. The effects of the resolution, however, are less systematic, which seem to be dependent on the range of structural wavelength considered.

Acknowledgments

The authors wish to acknowledge a grant from Research Grants Council of Hong Kong Special Administrative Region, China (PolyU 152026/14E).

References

Ang, Y. L., Koh, Y. K. and Lee, P. H. [2016] "Acoustic metamaterials: A potential for cabin noise control in automobiles and armed vehicles," *International Journal of Applied Mechanics* **8**, 1650072.

Bardell, N. S. [1991] "Free-vibration analysis of a flat-plate using the hierarchical finite-element method," *Journal of Sound and Vibration* **151**(2), 263–289.

Berry, A., Guyader, J. L. and Nicolas, J. [1992] "A general formulation for the sound radiation from rectangular, baffled plates with arbitrary boundary-conditions — Reply to comment," *Journal of the Acoustical Society of America* **92**(5), 2991–2992.

Beslin, O. and Nicolas, J. [1997] "A hierarchical functions set for predicting very high order plate bending modes with any boundary conditions," *Journal of Sound and Vibration* **202**(5), 633–655.

Carrie, C. and Webb, J. P. [1997] "Hierarchal triangular edge elements using orthogonal polynomials," *IEEE Antennas and Propagation Society International Symposium 1997*, Vols. 1–4, 1310–1313.

Castrillon-Candas, J. E. and Amaratunga, K. [2003] "Spatially adapted multiwavelets and sparse representation of integral equations on general geometries," *SIAM Journal on Scientific Computing* **24**(5), 1530–1566.

Chen, K. [1998] "On a class of preconditioning methods for dense linear systems from boundary elements," *SIAM Journal on Scientific Computing* **20**(2), 684–698.

Chen, W. S., You, X. G., Fang, B., Tang, Y. Y. and Huang, J. [2006] "Wavelet natural boundary element method for the Neumann exterior problem of Stokes equations," *International Journal of Wavelets Multiresolution and Information Processing* **4**(1), 23–39.

Cheng, L. and Lapointe, R. [1995] "Vibration attenuation of panel structures by optimally shaped viscoelastic coating with added weight considerations," *Thin-Walled Structures* **21**(4), 307–326.

Cheng, L. and Nicolas, J. [1992] "Free-vibration analysis of a cylindrical-shell circular plate system with general coupling and various boundary-conditions," *Journal of Sound and Vibration* **155**(2), 231–247.

Cohen, A. [2003] *Numerical Analysis of Wavelet Methods* (Elsevier, Amsterdam).

Daubechies, I. [1992] *Ten Lectures on Wavelets* (Society for Industrial and Applied Mathematics, Philadelphia).

de Lautour, N. J. [1999] "A Galerkin method for the numerical analysis of diffraction by a rectangular screen," *Journal of the Acoustical Society of America* **106**(6), 3072–3080.

Ford, J. and Chen, K. [2001] "Wavelet-based preconditioners for dense matrices with non-smooth local features," *BIT* **41**(2), 282–307.

Gantumur, T. and Stevenson, R. P. [2006] "Computation of singular integral operators in wavelet coordinates," *Computing* **76**(1–2), 77–107.

Geng, J., Zhang, X. W. and Chen, X. F. [2017] "High-frequency vibration analysis of thin plate based on wavelet-based FEM using B-spline wavelet on interval," *Science China* **60**(5), 792–806.

Langley, R. S. and Bardell, N. S. [1998] "A review of current analysis capabilities applicable to the high frequency vibration prediction of aerospace structures," *Aeronautical Journal* **102**(1015), 287–297.

Leissa, A. W. [1973] "The free vibration of rectangular plates," *Journal of Sound and Vibration* **31**(3), 257–293.

Li, W. L. and Daniels, M. [2002] "A fourier series method for the vibrations of elastically restrained plates arbitrarily loaded with springs and masses," *Journal of Sound and Vibration* **252**(4), 768–781.

Mallat, S. G. [1999] *A Wavelet Tour of Signal Processing* (Academic Press, San Diego).

Marburg, S. [2002] "Six boundary elements per wavelength: Is that enough?" *Journal of Computational Acoustics* **10**(1), 25–51.

Mutinda, M. and Cristinel, M. [2015] "The wavelet finite element method in the dynamic analysis of a functionally graded beam resting on a viscoelastic foundation subjected to a moving load." *European Journal of Computational Mechanics* **24**(5), 171–209.

Niccoleau, F. C. G. A. and Vassilicos, J. C. [2014] "Wavelet analysis of wave motion," *International Journal of Applied Mechanics* **6**, 1450021.

Pan, G. W., Wang, K. and Gilbert, B. K. [2003] "On multiwavelet-based finite-element method." *IEEE Transactions on Microwave Theory and Techniques* **51**(1), 148–155.

Rao, S. S. [2007] *Vibration of Continuous Systems* (Wiley, Hoboken, N.J.).

Ruta, P. [1999] "Application of Chebyshev series to solution of non-prismatic beam vibration problems," *Journal of Sound and Vibration* **227**(2), 449–467.

Su, Z., Jin, G. Y., Wang, X. R. and Maio, X. H. [2015] "Modified Fourrier-Ritz approximation for the free vibration analysis of laminated functionally graded plates with elastic restraints," *International Journal of Applied Mechanics* **5**, 1550073.

Tausch, J. and White, J. [2003] "Multiscale bases for the sparse representation of boundary integral operators on complex geometry." *SIAM Journal on Scientific Computing* **24**(5), 1610–1629.

Tran, T., Stephan, E. P. and Zaprianov, S. [1998] "Wavelet-based preconditioners for boundary integral equations," *Advances in Computational Mathematics* **9**(1–2), 233–249.

Zhang, S. and Cheng, L. [2015] "Shape optimization of acoustic enclosures based on a wavelet–Galerkin formulation," *International Journal of Applied Mechanics* **7**, 1550009.

Zhang, S. and Cheng, L. [2016] "On the efficacy of the wavelet decomposition for high frequency vibration analyses," *Journal of Sound and Vibration* **380**, 213–223.

Zheng, H. and Wei, Z. P. [2013] "Vibroacoustic analysis of stiffened plates with nonuniform boundary conditions," *International Journal of Applied Mechanics* **5**, 1350046.

Zhou, C. W., Laine, J. P., Ichchou, M. N. and Zine, A. M. [2015] "Wave finite element method based on reduced model for one-dimensional periodic structures," *International Journal of Applied Mechanics* **7**, 1550018.

Zhou, T., Tang, L. L., Ji, H. L., Qiu, J. H. and Cheng, L. [2017] "Dynamic and static properties of double-layered compound acoustic black hole structures," *International Journal of Applied Mechanics* **9**, 1750074.